Chemical Engineering Journal 143 (2008) 210–219

Contents lists available at ScienceDirect

Chemical Engineering Journal

journal homepage: www.elsevier.com/locate/cej

Thermodynamic analysis of a reactive distillation process for deep hydrodesulfurization of diesel: Effect of the solvent and operating conditions

Amado S. Granados-Aguilar [b], Tomás Viveros-García [a,*], Eduardo S. Pérez-Cisneros [a]

[a] Departamento de Ingeniería de Procesos e Hidráulica, Universidad Autónoma Metropolitana-Iztapalapa, San Rafael Atlixco 186, C.P. 09340, México, D.F., Mexico
[b] Departamento de Matemáticas, Facultad de Química, Universidad Nacional Autónoma de México, Ciudad Universitaria, C.P. 04510, México, D.F., Mexico

ARTICLE INFO

Article history:
Received 21 August 2007
Received in revised form 25 March 2008
Accepted 10 April 2008

Keywords:
Deep HDS of diesel
Reactive distillation
Effect of solvent

ABSTRACT

The effect of the solvent type, operating pressure and catalyst loading for deep hydrodesulfurization of diesel through a reactive distillation process has been analyzed. The analysis considers the computation of reactive residue curve maps for the hydrodesulfurization of dibenzothiophene (DBT) and 4,6-dimethyldibenzothiophene (4,6-DMDBT) in a simple reactive batch distillation process. For the computation of the reactive residue curves, the hydrogenolysis and hydrogenation reaction paths were considered. The visualization of the reactive residue curves is posed in terms of *elements*. Through the computation of the reactive residue curve maps it was possible to reproduce the experimental information stating that DBT is preferentially converted following the hydrogenolysis reaction route, while 4,6-DMDBT is mostly eliminated by the hydrogenation reaction route. From the reactive residue curve maps the effect of the solvent, pressure and catalyst loading on the conversion of 4,6-DMDBT was studied. It was found that when *n*-hexadecane (n-$C_{16}H_{34}$) is used as the solvent medium and the operating pressure is set to 10 atm a complete conversion of 4,6-DMDBT is achieved. The same conversion is achieved using tetraline ($C_{10}H_{12}$) as solvent but the pressure must be increased up to 30 atm and a higher amount of catalyst is required.

1. Introduction

Conventional hydrotreating is a commercially proven refining process in which a mixture of heated feedstock and hydrogen goes through a catalytic reactor to remove sulfur and other undesirable impurities. A review of the technologies for producing ultra-low sulfur diesel fuel (ULSD) reveals that current technologies can be modified to produce diesel with less than 10 parts per million (ppm) sulfur. Nevertheless, only a small number of refineries produce diesel with sulfur in the 10 ppm range on a limited basis. The existence of the required technology does not ensure, however, that all refineries will have that technology in place and in time to meet the new ULSD standards because these plants are characterized by a wide range of size, complexity, and quality of crude oil inputs.

Considerable development in reactor design and catalyst improvement has already been made to achieve ULSD levels near or below 10 ppm. In some cases low sulfur levels are the consequence of refiners' efforts to meet other specifications, such as the aromatic levels required in Scanraff, Sweden, where the refinery operates based on SynTechnology principles [1]. The Scanraff hydrotreating unit consists of an integrated two-stage reactor system with an interstage high-pressure gas stripper. The unit processes a light gas oil to produce a diesel product with less than 1 ppm sulfur and 2.4 vol.% aromatics. It is important to note that the Scanraff plant is highly selective of its feedstock to achieve the ultra-low sulfur content which may not be generalized to most refineries.

It is generally believed that a two-stage deep desulfurization process will be required by most, if not all refineries, to achieve a diesel product with less than 10 ppm sulfur. A design consistent with this technological approach is proposed by Haldor Topsøe [2], which includes a first stage that reduces the sulfur content to around 250 ppm or lower and a second stage that completes the reduction to less than 10 ppm. The DOE/EIA Report [2] points

Abbreviations: **A**, element A: organic part of the organosulfur compound; **B**, element B: sulfur atom; **C**, element C: hydrogen molecule; **D**, element D: solvent tetraline or *n*-hexadecane; **AB**, molecule AB: di-benzothiophene or 4,6-dimethyldibenzothiophene; **AC**, molecule AC: bi-phenyl or 3,3′-dimethylbiphenyl; **AC_4**, molecule AC_4: cyclohexylbenzene or 3-methylcyclohexyltoluene; **CB**, molecule CB: hydrogen sulfide; HDS, hydrodesulfurization; BPH, biphenyl; DBT, di-benzothiophene; 3,3′DMBPH, 3,3′-dimethylbiphenyl; 4,6-DMDBT, 4,6-dimethyldibenzothiophene; 3-MCHT, 3-methylcyclohexyltoluene; CHB, cyclohexylbenzene.

* Corresponding author. Tel.: +52 55 58 04 46 48; fax: +52 55 58 04 49 00.
E-mail address: tvig@xanum.uam.mx (T. Viveros-García).

1385-8947/$ – see front matter © 2008 Elsevier B.V. All rights reserved.
doi:10.1016/j.cej.2008.04.024

Nomenclature

C_i	is the concentration of species i
$k_{i,j}$	apparent reaction rate constant for species i in catalytic sites j
$K_{i,j}$	adsorption parameter for species i in catalytic sites j
L	molar liquid hold-up (kmol)
M_{cat}	catalyst mass (kg)
$r_{DBT,\sigma}$	DBT reaction rate at σ catalytic sites (kmol/kg cat. h)
$r_{DBT,\tau}$	DBT reaction rate at τ catalytic sites (kmol/kg cat. h)
r_0	reference rate of reaction (1×10^{-7} kmol/kg cat. h)
$r_{4,6\text{-DMDBT},\sigma}$	4,6-DMDBT reaction rate at σ catalytic sites (kmol/kg cat. h)
$r_{4,6\text{-DMDBT},\tau}$	4,6-DMDBT reaction rate at τ catalytic sites (kmol/kg cat. h)
$\bar{V}$	molar vapor flow rate (kmol/h)
W_j	*element* fraction for *element* j
x_i	liquid mole fraction of specie i

Greek symbols

α	dimensionless reaction-separation parameter
τ	"warped" time

out that, in some cases the first stage could be a conventional hydrotreating unit with moderate adjustments to the operation parameters, just as the higher activity catalysts for achieving a higher sulfur removal rate. The second stage requires substantial modification of the desulfurization process, primarily through higher pressure, increasing hydrogen flow rate and purity, reducing space velocity, and the appropriate selection of the catalyst. Knudsen et al. [3] suggested that to deep desulfurize cracked stocks, a higher operating pressure of the reactor is necessary. Pressure requirements would depend on the quality of the crude oil and the setup of the individual refinery, thus, the level of pressure required for deep desulfurization is a key uncertainty in assessing the cost and availability of the technology.

In a previous work, Viveros-García et al. [4] obtained a conceptual design of a reactive distillation column based on a thermodynamic analysis for DBT hydrodesulfurization reaction, considering the differences in volatility and reactivity between the organosulfur compounds. The conceptual design was based on the computation of the reactive residue curves map for DBT elimination. It was found that there exists a temperature region where the elimination of H_2S via vaporization was favored. Also, it could be found through rigorous simulations that reactive distillation could be a viable alternative to eliminate the heavier sulfur compounds present in the diesel at 30 atm.

In the present work, following the same approach, the thermodynamic analysis for sulfur elimination of DBT and the more recalcitrant compound 4,6-DMDBT in a simple reactive distillation process has been performed. As it was mentioned above, some of the difficulties encountered in the development of new HDS processes are the uncertainty in the level of pressure and catalyst loading required for deep desulfurization of different feedstocks. Therefore, the effect of the operating pressure, solvent medium and catalyst loading on the reactive residue curves maps are studied. The effect of these three parameters on the behavior of the reactive system is very important in order to obtain a reliable design of any reactive distillation column. For the computation of the reactive residue curves, both, the hydrogenolysis and hydrogenation reaction paths are considered. The visualization of the reactive residue curves is posed in terms of *elements* [5]. The thermodynamic properties for the organosulfur compounds not reported in the literature are predicted through the group contribution method of Joback and Reid [6].

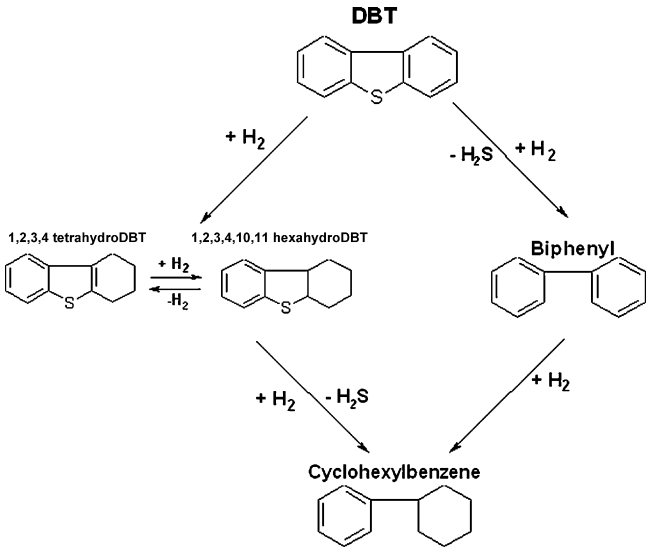

Fig. 1. Reaction pathways for dibenzothiophene hydrodesulfurization.

2. The HDS reactive system and the *element* approach

In general, there are two possible reaction paths for sulfur removal from the organosulfur compounds, as illustrated for dibenzothiophene (DBT), and 4,6-dimethyldibenzothiophene (4,6-DMDBT) in Figs. 1 and 2, respectively. The first route is the sulfur atom direct elimination (hydrogenolysis) from the sulfured molecule. The second route is the hydrogenation of one aromatic ring followed by the sulfur atom elimination.

The liquid phase hydrodesulfurization reactions for dibenzothiophene and 4,6-dimethyldibenzothiophene have been thoroughly studied and revisited by several authors [7,8]. The reaction network for dibenzothiophene hydrodesulfurization proposed by Houalla et al. [9] shown in Fig. 1, indicates two primary

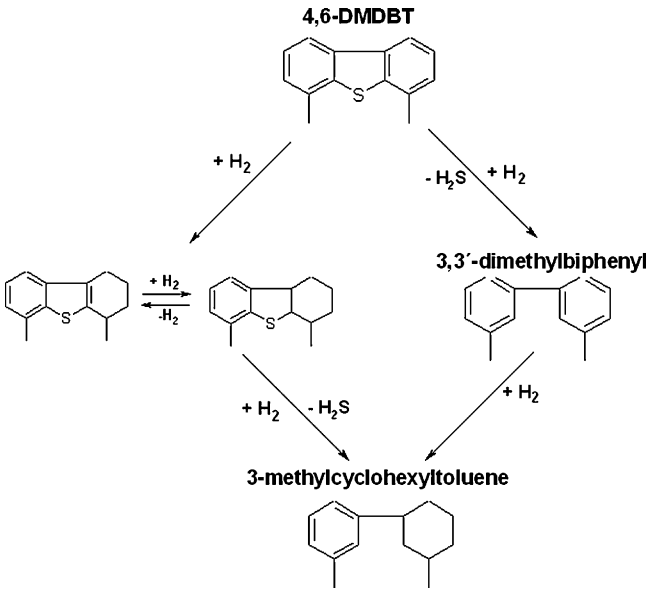

Fig. 2. Reaction pathways for 4,6-dimethyldibenzothiophene hydrodesulfurization.

routes: hydrogenation of one aromatic ring gives an equilibrium mixture of 1,2,3,4-tetrahydrodibenzothiophene and 1,2,3,4,10,11-hexahydrodibenzothiophene; hydrodesulfurization of these two intermediates occurs rapidly to give cyclohexylbenzene (CHB). This combination of reactions is designated as the *hydrogenation path*. The second route, direct hydrodesulfurization of dibenzothiophene to give biphenyl (BPh) is referred as the *hydrogenolysis path*. Biphenyl reacts further with hydrogen to give cyclohexylbenzene, but this reaction is typically two orders of magnitude slower than the rate of dibenzothiophene hydrogenolysis [7].

For 4,6-dimethyldibenzothiophene hydrodesulfurization reactions, Vanrysselberghe et al. [8] have proposed the reaction network shown in Fig. 2. The hydrodesulfurization reaction network for 4,6-DMDBT (see Fig. 2) indicates that, in the hydrogenation route, the 4,6-DMDBT is hydrogenated into partially hydrogenated dimethyldibenzothiophenes prior to sulfur removal. These intermediates are highly reactive and they are directly desulfurized into 3-methylcyclohexyltoluene (3-MCHT) and hydrogen sulfide. The hydrogenolysis reaction route gives 3,3′-dimethylbiphenyl (3,3′DMBPh) and hydrogen sulfide. 3,3′DMBPh is then hydrogenated into 3-MCHT.

The experimental results of Vanrysselberghe et al. [8] have shown that 4,6-DMDBT is less converted and more hydrogenated prior to sulfur removal and DBT is the most reactive compound in the hydrogenolysis reaction route. In general, when alkyl substituents are attached to the carbon atoms adjacent to the sulfur atom, the rate for direct sulfur elimination is diminished whereas the sulfur removal rate via the hydrogenation route is relatively unaffected [10]. Co–Mo catalysts desulfurize primarily via the direct route, while the Ni–Mo catalysts do it via the hydrogenation route. The extent to which a given catalyst acts via one route or the other is determined by the H_2 and H_2S partial pressures and the hydrocarbon feed properties.

In agreement with the reaction networks described in Figs. 1 and 2, at least one of the following two unbalanced hydrogenolysis–hydrogenation reactions should be carried out:

$$\mathrm{DBT} + \mathrm{H_2} \rightarrow \mathrm{BPh} + \mathrm{CHB} + \mathrm{H_2S},$$

$$4,6\text{-DMDBT} + \mathrm{H_2} \rightarrow 3,3'\text{-DMBPh} + \text{3-MCHT} + \mathrm{H_2S} \quad (1)$$

where BPh, and 3,3′-DMBPh are the hydrogenolysis reaction products and CHB, and 3-MCHT are the hydrogenation reaction products, respectively. The above unbalanced reactions (Eq. (1)) can be written in a balanced form as

$$2\mathrm{C_{12}H_8S} + 7\mathrm{H_2} \rightarrow \mathrm{C_{12}H_{10}} + \mathrm{C_{12}H_{16}} + 2\mathrm{H_2S},$$

$$2\mathrm{C_{14}H_{12}S} + 7\mathrm{H_2} \rightarrow \mathrm{C_{14}H_{14}} + \mathrm{C_{14}H_{20}} + 2\mathrm{H_2S} \quad (2)$$

In the above reaction schemes, potential side reactions, as hydrogenation of biphenyls, cyclohexylbenzenes and cyclohexyltoluenes are considered negligible in comparison with the hydrogenolysis and hydrogenation of dibenzothiophenes [7,8].

2.1. Graphical visualization of the reactive space

For the analysis of the reactive system, hydrodesulfurization reactions of the various species given by Eq. (2), may be lumped into the following general reaction:

$$\nu_1(\mathrm{C_NH_M{-}S}) + \nu_2\mathrm{H_2} \rightarrow \nu_3(\mathrm{C_NH_M{-}H_2}) + \nu_4(\mathrm{C_NH_M{-}H_{[\nu_2+(\nu_5-1)]}}) + \nu_5\mathrm{H_2S} \quad (3)$$

where ν_i is the stoichiometric coefficient of compound i in the reactive mixture, $\mathrm{C_NH_M}$ is the organic part of the organosulfur compound, ($\mathrm{C_NH_M{-}H_2}$) and ($\mathrm{C_NH_M{-}H_{[\nu_2+(\nu_5-1)]}}$) are the hydrogenolysis and hydrogenation reaction products, respectively. It can be noted that the hydrogenolysis–hydrogenation reactions given by Eq. (3) involve nine different species including the solvent. Such reactions are carried out in a mixture of many hydrocarbons as solvent medium, for example, a paraffinic blend of C_{10}–C_{16}. The computation and visualization of the phase behavior of this multicomponent reactive mixture may be difficult. This is because of the complexity of the reactive mixture containing H_2 and H_2S, and the lack of experimental values for some thermodynamic properties of the organosulfur compounds.

In order to simplify the visualization of the reactive phase behavior, it is possible to manage the hydrogenolysis–hydrogenation reactions for each organosulfur compound separately. Assuming a reactive mixture with only one organosulfur compound (i.e., DBT) and an inert species as solvent (i.e., *n*-hexadecane), and using the *element* concept proposed by Pérez-Cisneros et al. [5], a reduction of the composition space is possible. Defining the following *element* representation: **A** = $\mathrm{C_NH_M}$; **B** = S and **C** = H_2, the generalized reaction (3) can be written as

$$\nu_1\mathbf{AB} + \nu_2\mathbf{C} \rightarrow \nu_3\mathbf{AC} + \nu_4\mathbf{AC_4} + \nu_5\mathbf{BC} \quad (4)$$

where **AC** and $\mathbf{AC_4}$ represent all products obtained in the hydrodesulfurization reactions from all the organosulfur compounds **AB** studied here. Furthermore, considering that these liquid phase chemical reactions are carried out in a solvent medium, such solvent is introduced as *element* **D**.

The general *element* matrix considering the two organosulfur compounds can be written as

	DBT ($\mathrm{C_{N=12}H_{M=8}S}$), 4,6-DMDBT ($\mathrm{C_{N=14}H_{M=12}S}$) (1)	H_2 (2)	BPh ($\mathrm{C_{N=12}H_{M=8}H_2}$) 3,3′-DMBPh ($\mathrm{C_{N=14}H_{M=12}{-}H_2}$) (3)	CHB ($\mathrm{C_{N=12}H_{M=8}H_8}$) 3-MCHT ($\mathrm{C_{N=14}H_{M=12}H_8}$) (4)	H_2S (5)	Solvent (6)
A = $\mathrm{C_NH_M}$	ν_1	0	ν_3	ν_4	0	0
B = S	ν_1	0	0	0	ν_5	0
C = H_2	0	ν_2	ν_3	$4\nu_4$	ν_5	0
D = solvent	0	0	0	0	0	1

The *element* fractions (amount of *element j*/total amount of *elements*) are given as [5]:

$$W_A = \frac{\nu_1x_1 + \nu_3x_3 + \nu_4x_4}{2(\nu_1x_1 + \nu_3x_3 + \nu_5x_5) + \nu_2x_2 + 5\nu_4x_4 + x_6} \quad (5)$$

$$W_B = \frac{\nu_1x_1 + \nu_5x_5}{2(\nu_1x_1 + \nu_3x_3 + \nu_5x_5) + \nu_2x_2 + 5\nu_4x_4 + x_6} \quad (6)$$

$$W_C = \frac{\nu_2x_2 + \nu_3x_3 + 4\nu_4x_4 + \nu_5x_5}{2(\nu_1x_1 + \nu_3x_3 + \nu_5x_5) + \nu_2x_2 + 5\nu_4x_4 + x_6} \quad (7)$$

$$W_D = \frac{x_6}{2(\nu_1x_1 + \nu_3x_3 + \nu_5x_5) + \nu_2x_2 + 5\nu_4x_4 + x_6} \quad (8)$$

where x_i are the corresponding component mole fractions. The stoichiometric coefficients indicated in the *element* matrix for the two hydrodesulfurization reactions are $\nu_1 = 2$, $\nu_2 = 7$, $\nu_3 = 1$, $\nu_4 = 1$, $\nu_5 = 2$. The three-dimensional reactive space for all sulfur compounds in terms of the *elements* defined previously is shown in Fig. 3. The shadowed areas correspond to the two-dimensional reactive zones.

With the above *element* fraction definition, the nine different species participating in the hydrodesulfurization reactions are located in this reactive phase diagram. Also, if the solvent concentration is kept constant (W_D = constant), different normalized planes for the reactive mixture could be sketched (see upper plane in Fig. 3). The solvent-free coordinates in the reactive diagram for

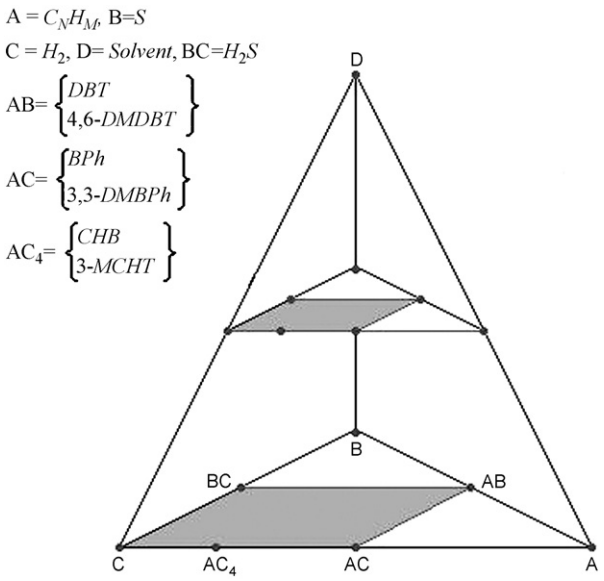

Fig. 3. Three-dimensional *element* composition space for HDS of diesel.

the pure species are

$$\mathbf{AB} = \left\{ \begin{matrix} \text{DBT} \\ \text{4, 6-DMDBT} \end{matrix} \right\} = (W_A,\ W_B,\ W_C) = (0.5, 0.5, 0.0)$$

$$\mathbf{AC} = \left\{ \begin{matrix} \text{BPh} \\ \text{3, 3′-DMBPh} \end{matrix} \right\} = (W_A,\ W_B,\ W_C) = (0.5, 0.0, 0.5)$$

$$\mathbf{AC_4} = \left\{ \begin{matrix} \text{CHB} \\ \text{3 – MCHT} \end{matrix} \right\} = (W_A,\ W_B,\ W_C) = (0.2, 0.0, 0.8)$$

$$\mathbf{BC} = \{\text{H}_2\text{S}\} = (W_A,\ W_B,\ W_C) = (0.0, 0.5, 0.5)$$

$$\mathbf{C} = \{\text{H}_2\} = (W_A,\ W_B,\ W_C) = (0.0, 0.0, 1.0)$$

Fig. 4 shows the normalized triangular phase diagram for the hydrogenolysis–hydrogenation reactions with a constant solvent concentration or without solvent. Thick lines in Fig. 4 indicate the reactive zone boundaries, thus, any point outside these boundaries

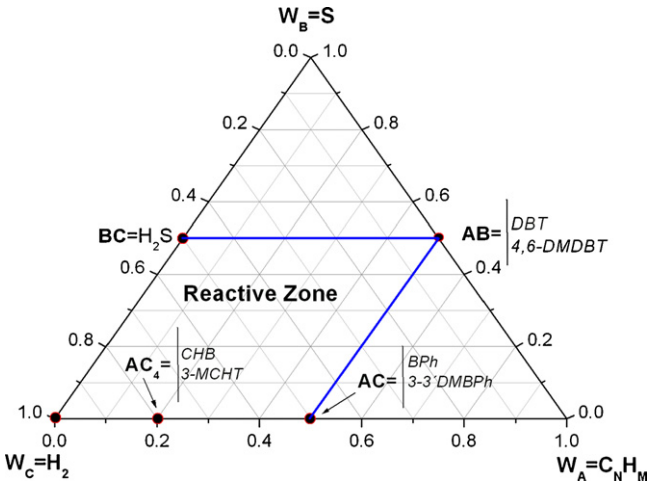

Fig. 4. Normalized triangular reactive composition diagram with constant solvent compositions (W_D = constant) or solvent free.

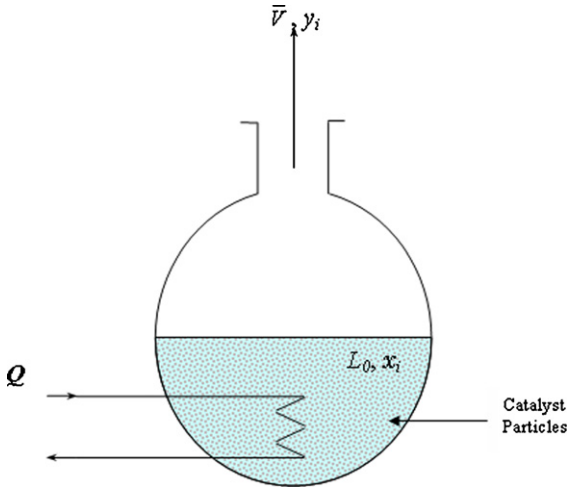

Fig. 5. Simple reactive batch distillation process.

does not belong to the reactive space of the reactive separation process.

3. The simple reactive distillation process

Considering a simple non-reactive batch distillation process shown in Fig. 5 (assuming no catalyst present), the component mass balances can be written as

$$\frac{dx_i}{dt} = \frac{\bar{V}}{L}(x_i - y_i) \tag{9}$$

where the molar liquid hold-up is L and $\bar{V}$ is the molar vapor flow rate. The quotient $L/\bar{V}$ is controlled via the heating input Q, and in this case it may be assumed that the heating strategy is such that

$$\frac{L}{\bar{V}} = \frac{L_0}{\bar{V}_0} = \text{constant} \tag{10}$$

This heating policy is physically significant and it leads to an autonomous ordinary differential equations model [11]. Substitution of Eq. (10) in Eq. (9) gives

$$\frac{dx_i}{d\tau} = (x_i - y_i); \quad \text{with} \quad d\tau = \frac{L_0}{\bar{V}_0}\,dt \tag{11}$$

Eq. (11) represents the variation of the liquid composition in the still, when no reaction is occurring, with respect to a "warped" time τ. It is clear that, as the time is running, the liquid composition in the pot will be richer in the heaviest compounds since the most volatile species will leave out with the vapor flow. By the sequential integration of Eq. (11) a set of equilibrium composition points are obtained and the resulting curve that describes the liquid composition is called a *non-reactive residue curve*. The equations to compute the *reactive* residue curves are similar to those for the non-reactive case, but, the reaction term must be added into the mass balances and a reaction kinetic expression has to be used to compute such curves. The autonomous differential equations for computation of the reactive residue curves can be written as

$$\frac{dx_i}{d\tau} = x_i - y_i + \alpha \sum_{j=1}^{NR} \left\{ \left[\nu_{ij} - \left(\sum_{k=1}^{NC} \nu_{kj} \right) x_i \right] \frac{r_j}{r_0} \right\} \tag{13}$$

where α is a dimensionless reaction-separation parameter given by

$$\alpha = \frac{M_{cat} r_0}{\bar{V}_0} \tag{14}$$

Table 1
Physical properties for some organosulfur compounds present in the diesel

Compound	T_m (K)	T_b (K)	T_c (K)	Pc (atm)	ω
Dibenzothiophene	415.05	587.98	853.65	37.59	0.484
4,6-Dimethyldibenzothiophene	462.63	643.70	898.94	29.12	0.584
Biphenyl	277.34	527.32	777.19	34.28	0.377
3,3′-Dimethylbiphenyl	324.92	583.04	824.77	26.85	0.474
Cyclohexylbenzene	258.30	520.19	760.98	29.73	0.354
3-Methylcyclohexyltoluene	289.12	566.26	798.79	23.25	0.423

Properties computed from Joback and Reid Group Contribution Method [6].

In Eq. (13) NC is the number of components participating in reaction j, NR is the number of reactions, M_{cat} is the catalyst mass (kg), $\bar{V}_0$ is the vaporization flow rate (kmol/h), r_j is the intrinsic rate of reaction j (kmol/kg cat. h), r_0 is a reference rate of reaction (in this work 1×10^{-7} kmol/kg cat. h) and ν_{ij} is the stoichiometric coefficient of compound i in reaction j. The reaction-separation parameter α indicates the ratio between the amounts of catalyst loaded in the distillation vessel (i.e., total wetted reacting area) multiplied by the reference rate of reaction to the vaporization flow rate. It should be clear that, in the mathematical model (Eq. (13)) it is assumed that there are no diffusion limitations of the reactants. To carry out the integration of Eq. (13) it is necessary to calculate (i) the phase equilibrium and (ii) the reaction terms. One of the problems in the phase equilibrium calculations for the hydrodesulfurization reactive system is the lack of experimental information of the critical properties and acentric factors for 4,6-DMDBT compound and its respective hydrogenolysis and hydrogenation reaction products. In the present work, the critical properties and acentric factors were estimated using the Joback and Reid method [6] for DBT and 4,6-DMDBT, and their respective hydrogenolysis and hydrogenation reaction products. These properties are shown in Table 1.

With these estimated properties it is possible to compute the required fugacity coefficients and to determine the phase equilibrium behavior of the reactive mixture the original Peng–Robinson equation of state [12] with the appropriate binary interaction coefficients was used. In order to avoid trivial solutions, the phase stability test procedure proposed by Michelsen [13] was applied. It should be pointed out that such stability test was needed since the certainty on the existence of the involved phases is required.

For the computation of the reaction terms in Eq. (13), the kinetic models for hydrogenolysis (σ catalytic sites) and hydrogenation (τ catalytic sites) reactions of dibenzothiophene, and alkyl substituted dibenzothiophenes reported by Broderick and Gates [7] and Vanrysselberghe et al. [8], respectively, were used. That is

- For dibenzothiophene:

$$r_{DBT,\sigma} = \frac{k_{DBT,\sigma} K_{DBT,\sigma} K_{H_2,\sigma} C_{DBT} C_{H_2}}{(1 + K_{DBT,\sigma} C_{DBT} + K_{H_2S,\sigma} C_{H_2S})^2 (1 + K_{H_2,\sigma} C_{H_2})} \quad (15)$$

$$r_{DBT,\tau} = \frac{k_{DBT,\tau} K_{DBT,\tau} K_{H_2,\tau} C_{DBT} C_{H_2}}{1 + K_{DBT,\tau} C_{DBT}} \quad (16)$$

- And for 4,6-dimethyldibenzothiophene:

$$r_{4,6\text{-DMDBT},\sigma} = \frac{k_{4,6\text{-DMDBT},\sigma} K_{4,6\text{-DMDBT},\sigma} K_{H_2,\sigma} C_{4,6\text{-DMDBT},\sigma} C_{H_2}}{\left(1 + K_{4,6\text{-DMDBT},\sigma} C_{4,6\text{-DMDBT}} + \sqrt{K_{H_2,\sigma} C_{H_2}}\right)^3} \quad (17)$$

$$r_{4,6\text{-DMDBT},\tau} = \frac{k_{4,6\text{-DMDBT},\tau} K_{4,6\text{-DMDBT},\tau} K_{H_2,\tau} C_{4,6\text{-DMDBT},\tau} C_{H_2}}{\left(1 + K_{4,6\text{-DMDBT},\tau} C_{4,6\text{-DMDBT}} + \sqrt{K_{H_2,\tau} C_{H_2}}\right)^3} \quad (18)$$

where k_{ij} is the apparent reaction rate constant for species i in catalytic sites j, K_{ij} is the adsorption parameter for species i in catalytic sites j and C_i is the concentration of species i. Appendix A shows the temperature dependency of all parameters used in Eqs. (15)–(18).

4. The reactive residue curves maps

In this work, the "sulfured" diesel has been considered as a solvent-rich mixture, since the composition of DBT or 4,6-DMDBT is equivalent to 500 wppm. Experimental results on hydrodesulfurization kinetics have been reported measuring the reaction rates for DBT or 4,6-DMDBT with hydrogen and a solvent. Commonly employed solvents for such experimental hydrodesulfurization reactions are *n*-hexadecane [7,9], a mixture of *n*-paraffins [8] or decaline [14–17]. According with the above, in this work tetraline (1,2,3,4-tetrahydronaphtalene) and *n*-hexadecane were selected as the solvent media. Tetraline is a product of naphtalene hydrogenation and, together with *n*-hexadecane, it may be considered that it is present in a "real" diesel mixture. To compute the non-reactive and reactive residue curves, an initial point close to the left corner on the triangular diagram was chosen. This initial point represents the composition of a "sulfured" diesel with mole fractions: 0.0005 for DBT or 4,6-DMDBT (**AB**), 0.005 for H_2 (**C**) and 0.9945 for tetraline (**D**), and it is assumed that no reaction products are present. These initial mole fractions correspond to the following *element* fractions: $W_A^{0*} = W_B^{0*} = 9.695 \times 10^{-4}$; $W_C^{0*} = 3.393 \times 10^{-2}$; $W_D^{0*} = 0.96413$, and their normalization (considering constant $W_D^{0*} = 0.96413$) gives $W_A^0 = W_B^0 = 0.02703$; $W_C^0 = 0.94594$ (see Fig. 6). These normalized *element* fractions allow to locate the initial point in the element phase diagram near to the **C** node (pure H_2). The proposed initial value is the same for all calculations performed onward.

4.1. Non-reactive residue curves

Fig. 6 shows the non-reactive residue curve for a DBT–H_2–tetraline mixture obtained by the sequential integration of Eq. (11). It is important to notice that, because the DBT liquid mole fraction is so small, its effect on the phase equilibrium calculations is not considerable. Therefore, the non-reactive phase equilibrium behavior is not dependent on the organosulfur compound, thus the path of the non-reactive residue curve is virtually the same, and independent of the organosulfur reactant considered. In other words, the organosulfur compound in Fig. 6,

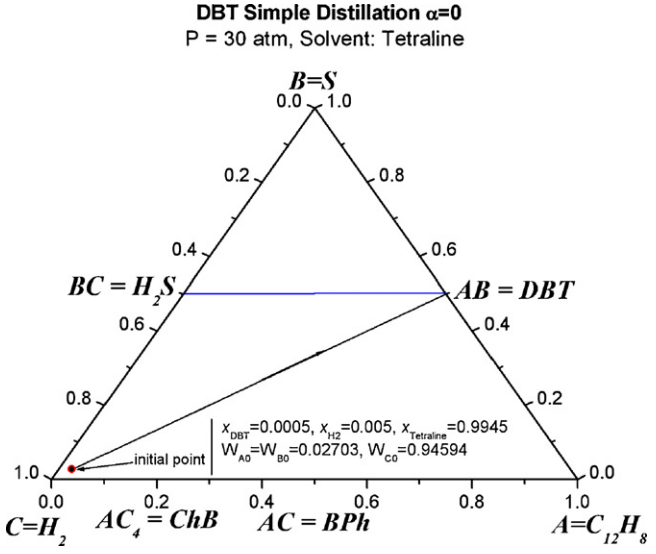

Fig. 6. Non-reactive residue curve for DBT.

AB, could be anyone, DBT or 4,6-DMDBT, and through a simple distillation (no catalyst present), a straight line pointing to the organosulfur compound is obtained.

It can be observed in Fig. 6 that the non-reactive residue curve leads to the **AB** stable node, which corresponds to the heaviest compound present in the initial mixture. This is an expected behavior when the initial mixture is vaporized without chemical reaction in the heated still.

4.2. Reactive residue curves

The reactive residue curves are obtained by the sequential integration of Eq. (13). In this case an amount of catalyst is loaded ($\alpha \neq 0$) in the still and the HDS reactions are carried out. In order to visualize the effect of the chemical reactions on the phase equilibrium behavior, each HDS reaction pathway was analyzed separately. That is, first, it was considered that only the single hydrogenolysis or hydrogenation reaction route was occurring and, afterwards, both reaction routes were simultaneously carried out. The set of reactive residue curve maps shown in Figs. 7 and 8 were computed considering an operating pressure of 30 atm and several catalyst loadings (different α values) were used. It should be noticed, in all these Figures, that the reactive residue curves are formed in two sections: (i) one section where reaction and separation are occurring simultaneously, and the reactive residue curve is drawn by broken lines describing the liquid phase composition in the reactive zone and (ii) the second section where only the simple distillation of the remaining mixture is carried out and the residue curve is drawn by continuous lines. Thick points (•) in the figures indicate the limits between the reactive and non-reactive (simple distillation) sections for each one of the residue curves computed. It should be noted that the simple distillation process lies over the lower reactive separation boundaries **AB**–**AC** or **AB**–**AC**$_4$, depending on the reaction route considered. Also, on the reactive residue curve maps, the boiling temperatures at the corresponding pressures (at 30 or 10 atm) are indicated below the pure components nodes.

4.2.1. Effect of the reaction route and catalyst loading (α) on the DBT and 4,6-DMDBT hydrodesulfurization

Reactive residue curve maps for a DBT–H_2–tetraline ($C_{10}H_{12}$) and 4,6-DMDBT–H_2–tetraline reacting mixtures under a hydrodesulfurization reactive distillation process were calculated. Fig. 7a–c shows the reactive residue curves corresponding to individual and simultaneous DBT hydrogenolysis and hydrogenation reactions at 30 atm, respectively. The employed α values were 0.05, 0.1, 0.5 and 2.0. Computed non-reactive ($\alpha = 0$) and reactive residue curves were plotted in an *element* ternary phase diagram at the same operating pressure.

A first observation of these reactive phase diagrams shows the expected modification of the reactive residue curves corresponding to each individual reaction path. Such modification corroborates the presence of the different HDS reaction products in the boiling reactive mixture, with their different *element* locations on the reactive phase diagrams.

A more detailed observation of the reactive phase diagram for DBT hydrogenolysis reaction (Fig. 7a) shows that the reactive residue curves deviate, from the non-reactive residue curve, toward the representative point of the hydrogenolysis organic product, biphenyl, or the *element* combination **AC**. This trend is proportionally accentuated as the α-value increases. It should be clear that the increment of α must be understood as an increment in the catalyst loading or a decrease in the liquid evaporation rate, $\bar{V}$, which represents an increment in the residence time of the reacting liquid mixture in the still. Therefore, for the higher registered α values (0.5 and 2.0), the corresponding reactive residue curves (broken lines) move

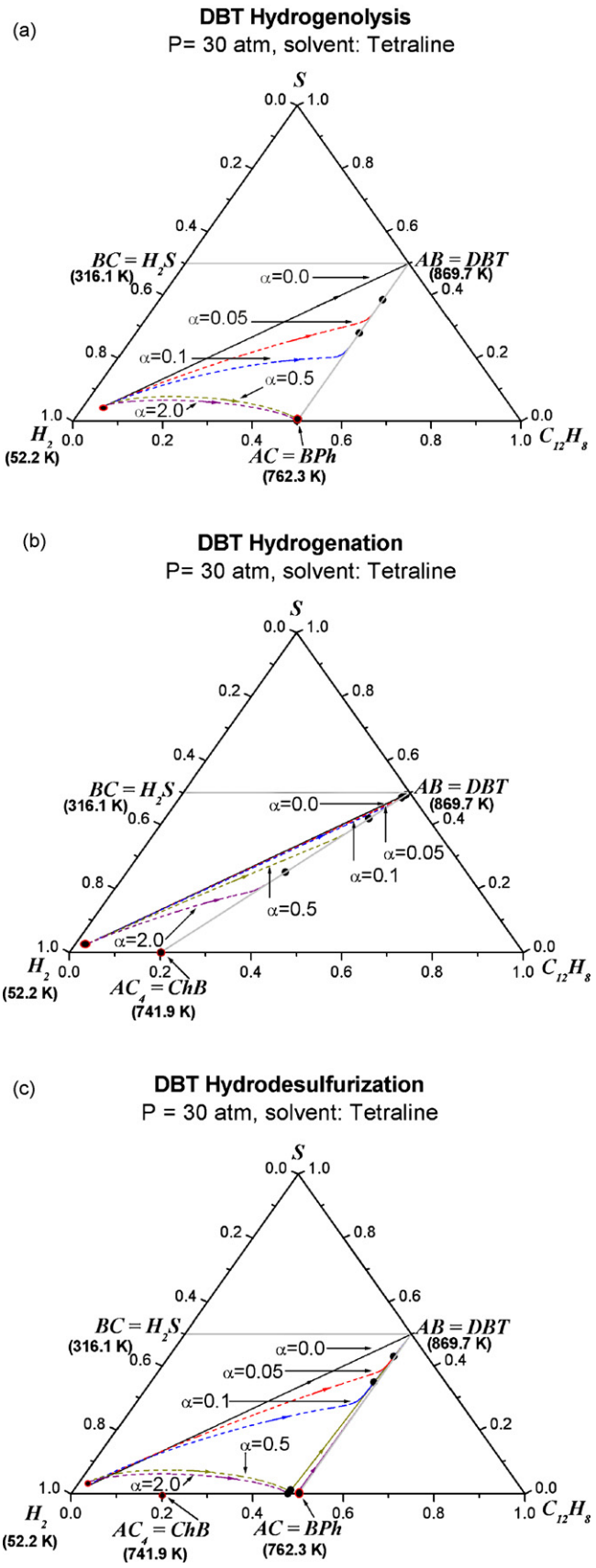

Fig. 7. (a) Reactive residue curves map for DBT hydrogenolysis; (b) reactive residue curves map for DBT hydrogenation; and (c) reactive residue curves map for DBT hydrodesulfurization.

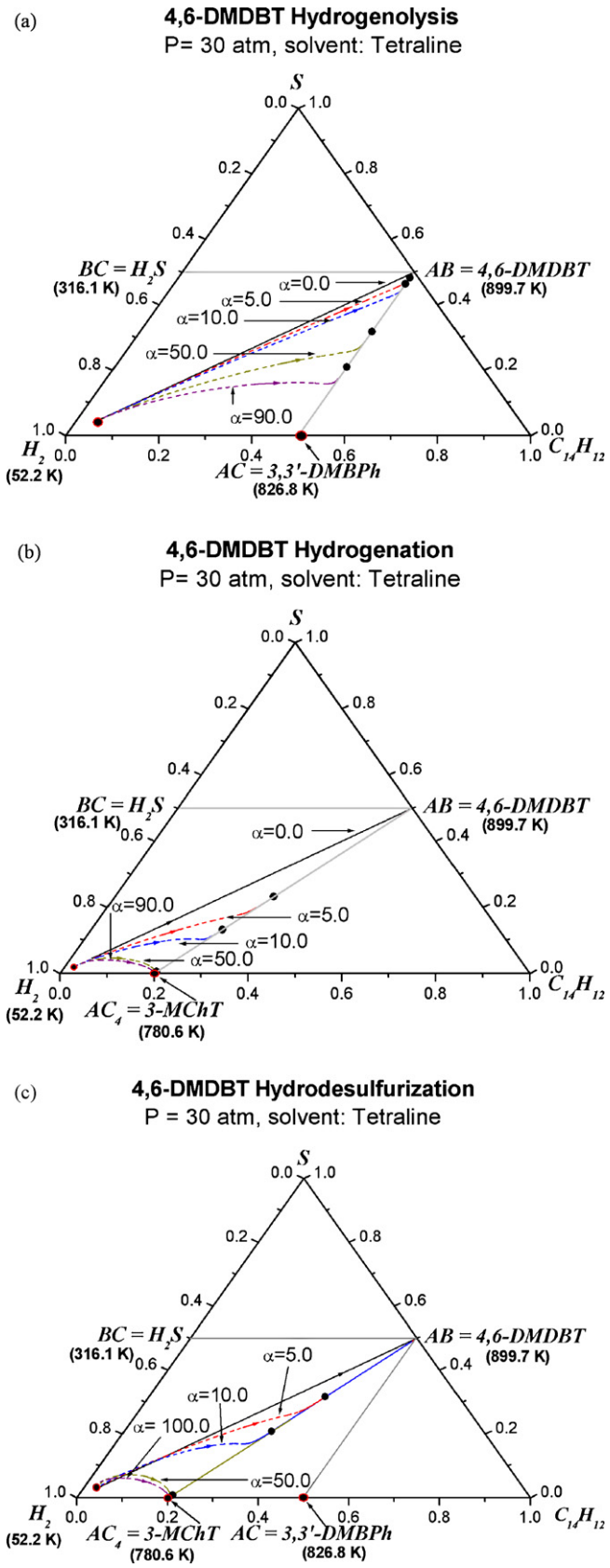

Fig. 8. (a) Reactive residue curves map for 4,6-DMDBT hydrogenolysis; (b) reactive residue curves map for 4,6-DMDBT hydrogenation; and (c) reactive residue curves map for 4,6-DMDBT hydrodesulfurization.

from the standardized initial point to the **AC** node. After that, a simple distillation of the DBT–biphenyl–tetraline mixture, is described on the reactive diagram by means of continuous lines. These continuous lines move over the reactive zone boundary line toward the **AB** node (pure DBT) independently of the value of α. Solid dots are used to indicate where the reactive curve section ends.

On the other hand, when the hypothetical individual hydrogenation reaction occurs (see Fig. 7b), the reactive residue curves do not show a noticeable trend toward the representative hydrogenation product point (cyclohexylbenzene) corresponding to the $\mathbf{AC}_4$ node. In other words, under the same reaction conditions (same α values), cyclohexylbenzene formation is significantly smaller compared to biphenyl formation. In fact, in the case that a complete elimination of DBT was required through this individual reaction path, a sensitive increment of the α-value should be done. The above is a very important result and it is consistent with the experimental work of Broderick and Gates [7], who concluded that for DBT hidrodesulfurization, the hydrogenolysis reaction path is mostly favored.

The combined effect of the simultaneous hydrogenolysis and hydrogenation reactions on the DBT–H_2–tetraline reactive mixture, can be analyzed in the reactive phase diagram shown in Fig. 7c. The reactive residue curves follow a similar trajectory to those found for the individual hydrogenolysis reaction route (see Fig. 7a). These curves move toward a point located on the base of the reactive phase diagram, closer to the **AC** node than to the $\mathbf{AC}_4$ node. It is clear that the hydrogenolysis reaction route is favored when the simultaneous action of the two chemical reactions routes occur, in spite of the H_2S production which, according to experimental information [7] inhibits mainly the hydrogenolysis reaction route.

It should also be noticed that continuous lines on the reactive phase diagram in Fig. 7c, corresponding to the non-reactive simple distillation process of DBT–biphenyl–cyclohexylbenzene–tetraline system, do not move over the reactive boundary line **AB**–**AC**, which represents a DBT–biphenyl–tetraline mixture, due to the presence of cyclohexylbenzene, although they move permanently toward the pure component DBT (**AB** *element* node).

Fig. 8a and b shows the behavior of the hypothetical individual hydrogenolysis and hydrogenation reactive distillation processes for 4,6-DMDBT, respectively. As in the previous case, dotted lines in reactive phase diagrams describe the behavior of the liquid phase in the reactive zones, continuous lines represent the simple distillation process and thick points indicate the limit of the reactive and non-reactive sections.

Fig. 8a shows that, for 4,6-DMDBT hydrogenolysis reaction route, despite the larger values of α used, in comparison to those for DBT, the reactive residue curves do not lead to the node **AC** (corresponding to the reaction product) in the reactive diagram. It can be observed that, in order to obtain representative conversions of 4,6-DMDBT, the α values should be increased 5 or 10 times ($\alpha = 50$, 90), compared to the values near to the non-reactive residue curve ($\alpha = 5, 10$); and in comparison to DBT case about 45–50 times higher. This result means that the amount of catalyst loaded in the still or the residence time of the reacting liquid mixture should be increased considerably, in order to obtain significant conversion levels of 4,6-DMDBT. Also, it indicates the need for more active catalysts to be developed.

On the other hand, Fig. 8b shows the representative reactive residue curves corresponding to a hypothetical 4,6-DMDBT hydrogenation reactive distillation process. It can be observed in Fig. 8b that the reactive residue curves trajectories substantially differ from those for DBT hydrogenation.

The reactive phase diagram in Fig. 8b shows that, for the same α values used in the hydrogenolysis route (see Fig. 8a), the reactive residue curves describe a clear trend toward the

AC$_4$ node, corresponding to the hydrogenation reaction product 3-methylcyclohexyltoluene. This behavior indicates that the hydrogenation reaction route is favored in the 4,6-DMDBT elimination. Also, it should be noticed that a small effect on the 4,6-DMDBT conversion is observed when the α-value is increased from 50 to 90, indicating that an increment in the amount of catalyst does not necessarily lead to a substantial conversion of 4,6-DMDBT.

Fig. 8c shows the reactive phase diagram when both hydrogenolysis and hydrogenation reactions routes are considered for 4,6-DMDBT elimination. It can be observed in Fig. 8c that, for the same α values, the trajectories of the reactive residue curves are similar to those for the hydrogenation reaction route. These results are in agreement with the experimental information stating that 4,6-DMDBT is preferentially eliminated through the hydrogenation reaction route [8]. It should be noted in Fig. 8c that the simple non-reactive distillation process occurs over the reactive boundary line **AC**$_4$–**AB**, corresponding to a non-reactive mixture of 4,6-DMDBT, 3-methylcyclohexyltoluene and tetraline.

4.2.2. Effect of the operating pressure on the 4,6-DMDBT hydrodesulfurization

The effect of the operating pressure on the 4,6-DMDBT hydrodesulfurization is shown in Fig. 9. It should be noted in Fig. 9 that both, hydrogenolysis and hydrogenation routes, are considered for the computation of the reactive residue curves at 10 atm. The comparison of Figs. 8c and 9 reveals that, when the pressure in the still decreases to 10 atm and tetraline is the solvent medium, an important decrement in 4,6-DMDBT conversion occurs. In fact, the reactive residue curves in the reactive phase diagram (see Fig. 9) for low α values (α = 5, 10) show a trend similar to that for the non-reactive residue curve, and only when the catalyst loading is largely increased (α = 200.0) a deviation to the reactions products is observed. The fall in 4,6-DMDBT conversion can be clearly observed in Fig. 10a and b, where the component mole fractions obtained from the reactive residues curve computation, for the liquid and vapor phases, are plotted versus temperature. It is clear that, the reduction of the operating pressure in the still, would lead to a reduction of the boiling temperatures of the reacting mixture as shown in Fig. 10b. It can be noted in Fig. 10a that for α = 200.0 and P = 30 atm, the complete elimination of 4,6-DMDBT occurs around T = 718 K, while for P = 10 atm (Fig. 10b) it never occurs for the entire temperature range explored. This effect could be explained through

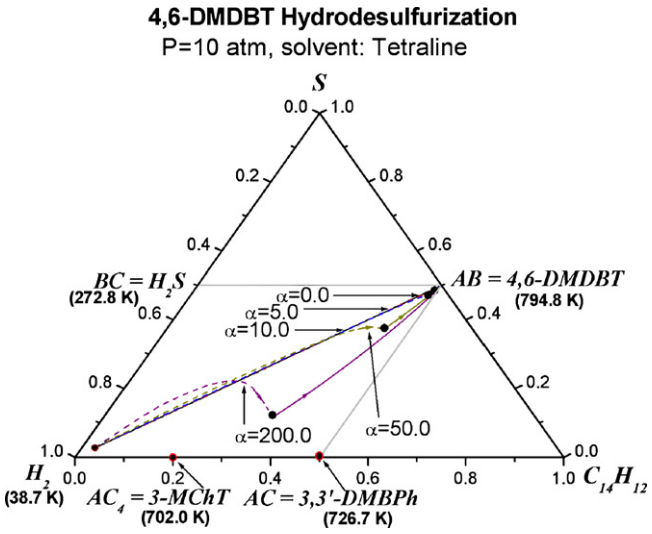

Fig. 9. Reactive residue curves map for 4,6-DMDBT hydrodesulfurization at 10 atm and tetraline as solvent.

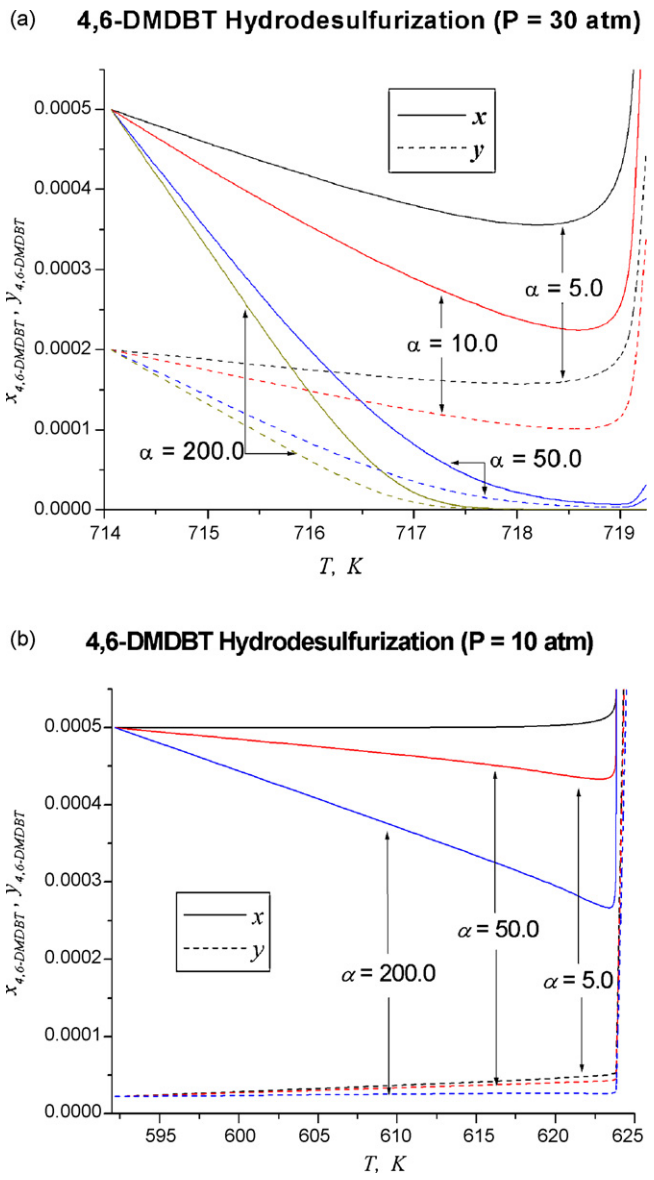

Fig. 10. Effect of the operating pressure on the conversion of 4,6-DMDBT: (a) P = 30 atm and (b) P = 10 atm.

the reduction of the hydrogen solubility due to the lower pressure. Based on the above, it is apparent that a reduction in the operating pressure would lead to a considerable decrease of the sulfur elimination from diesel.

4.2.3. Effect of the solvent on the 4,6-DMDBT hydrodesulfurization

As mentioned before, in the present work, two solvents, tetraline and hexadecane, were chosen as solvent medium. Fig. 11 shows the reactive residue curves map for 4,6-DMDBT hydrodesulfurization at P = 10 atm with hexadecane as solvent. It can be observed in Fig. 11 that the trend of the reactive residue curves points to the **AC**$_4$ node, indicating that, under these operating conditions, the conversion of 4,6-DMDBT is increased as the catalyst loading increases. It is shown that whereas a low conversion of 4,6-DMDBT was obtained with tetraline as solvent at 10 atm (see Fig. 10a), the switch to hexadecane as solvent leads to a complete elimination of 4,6-DMDBT with α = 800. This result indicates that although 4,6-DMDBT can be eliminated at a pressure of 10 atm a very large

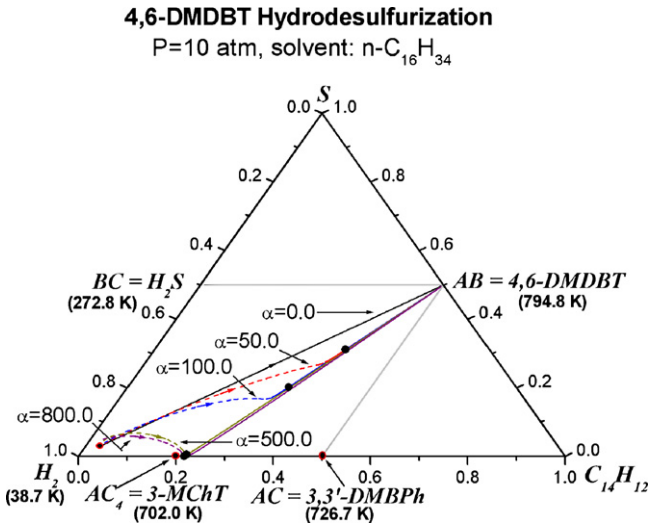

Fig. 11. Reactive residue curves map for 4,6-DMDBT hydrodesulfurization at 10 atm and *n*-hexadecane as solvent.

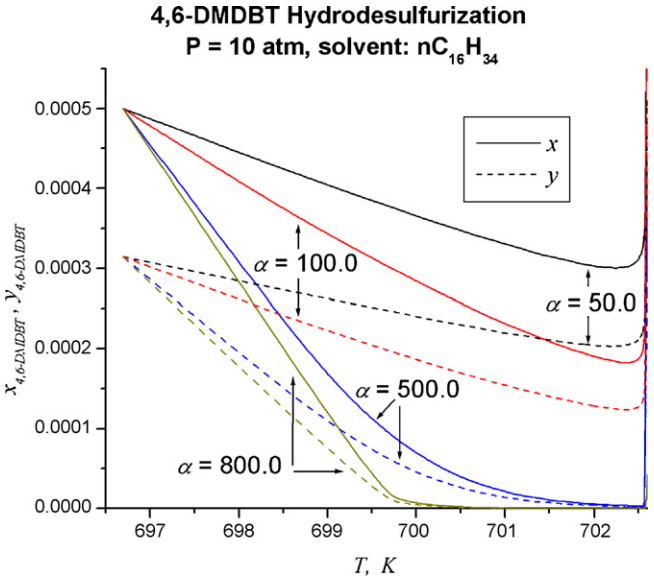

Fig. 12. Composition profile of 4,6-DMDBT at 10 atm and *n*-hexadecane as solvent medium.

amount of catalyst is required. Fig. 12 shows the component mole fractions for 4,6-DMDBT in both phases, indicating that complete elimination of 4,6-DMDBT occurs at $T = 702$ K for $\alpha = 500.0$, with the corresponding raise in the boiling temperatures of the reacting mixture when hexadecane is chosen as solvent. The above behavior may be explained through the increase of the hydrogen solubility in hexadecane. It is known from experimental information [18] that hydrogen solubility increases as the number of carbon atoms increases in the hydrocarbon chain. It is clear that, in order to have complete elimination of sulfur from diesel, a careful choice of the operating pressure and the solvent medium should be done.

5. Conclusions

The effect of the solvent, operating pressure and catalyst loading for deep hydrodesulfurization of diesel through a reactive distillation process has been analyzed. The thermodynamic analysis considers the computation of reactive residue curve maps for the hydrodesulfurization of dibenzothiophene (DBT) and 4,6-dimethyldibenzothiophene (4,6-DMDBT) in a simple reactive batch distillation process. Through the calculation of the reactive residue curve maps it was possible to reproduce the experimental information which indicates that DBT is preferentially converted through the hydrogenolysis reaction route, while 4,6-DMDBT is mostly eliminated by the hydrogenation reaction route. In the analysis of the reactive phase behavior the effect of the catalyst loading, operating pressure, and type of solvent were studied. From the reactive residue curve computation it could be observed that, using tetraline as solvent medium and reducing the operating pressure to 10 atm, a remarkable decrease in 4,6-DMDBT conversion occurs. This could be explained by the severe decrease of hydrogen concentration in the liquid phase due to the pressure reduction and consequently a lower solubility. However, if a combination of *n*-hexadecane as solvent and a low operating pressure (10 atm) is proposed, with the appropriate amount of catalyst load ($\alpha = 800$) a complete elimination of sulfur from diesel could be achieved. Nevertheless, this result indicates the employment of a large amount of catalyst, but also the need to develop more active and efficient catalysts for this process. It should be pointed out that, even when the results obtained through the calculation of the reactive residue curves indicate that reactive distillation could be a viable second stage process for deep HDS of diesel, there are uncertainties about the "true" critical properties of the HDS reactants and reaction products, which in this work were estimated by a group contribution method.

Acknowledgements

We thank CONACyT for the financial support through the project U45160-Y. S. Granados-Aguilar thanks CONACyT for the scholarship provided.

Appendix A. Apparent reaction rate constants and adsorption parameters used in Eqs. (15)–(18)

For DBT

$$k_{\mathrm{DBT},\sigma} = 7.87 \times 10^5 \exp\left(\frac{-1.26\times10^8}{R_g T}\right); \quad K_{\mathrm{DBT},\sigma} = 1.8 \times 10^{-1} \exp\left(\frac{1.9\times10^7}{R_g T}\right)$$

$$K_{\mathrm{H_2},\sigma} = 4.0 \times 10^3 \exp\left(\frac{3.5\times10^7}{R_g T}\right); \quad K_{\mathrm{H_2S},\sigma} = 7 \times 10^{-1} \exp\left(\frac{2.2\times10^7}{R_g T}\right)$$

$$k_{\mathrm{DBT},\tau} K_{\mathrm{H_2},\tau} = 4.22 \times 10^4 \exp\left(\frac{-1.16\times10^8}{R_g T}\right); \quad K_{\mathrm{DBT},\tau} = 2.0 \exp\left(\frac{6.0\times10^6}{R_g T}\right)$$

For 4,6-DMDBT

$$k_{\text{4,6-DMDBT},\sigma} = 6.44560 \times 10^7 \exp\left(\frac{-106223}{R_g T}\right); \quad K_{\text{4,6-DMDBT},\sigma} = 18.0397$$

$$K_{\mathrm{H_2},\sigma} = 3.36312 \times 10^{-11} \exp\left(\frac{113232}{R_g T}\right); \quad K_{\mathrm{H_2S},\sigma} = 1.47118 \times 10^{-8} \exp\left(\frac{105670}{R_g T}\right)$$

$$k_{\text{4,6-DMDBT},\tau} = 3.68208 \times 10^{27} \exp\left(\frac{-299042}{R_g T}\right); \quad K_{\text{4,6-DMDBT},\tau} = 1.58733 \times 10^{-8} \exp\left(\frac{90485}{R_g T}\right)$$

$$K_{\mathrm{H_2},\tau} = 1.40255 \times 10^{-15} \exp\left(\frac{142693}{R_g T}\right)$$

where T is in (K) and R_g is in (kJ/(kmol K))

References

[1] B. Van der Linde, R. Menon, D. Dave, S. Gustas, SynTechnology: an attractive solution for meeting future diesel specifications, in: Presented at the Asian Refining Technology Conference, ARTC, 1999.
[2] DOE/EIA Report, Energy Information Administration (EIA), Office of Integrated Analysis and Forecasting, The transition to ultra-low-sulfur diesel fuel: effects on prices and supply, U.S. Department of Energy, Washington, DC 20585, 2001, pp. 13–22.
[3] K.G. Knudsen, B.H. Cooper, H. Topsoe, Catalyst and process technologies for ultra low sulfur diesel, Appl. Catal.: Gen. 189 (1999) 205–215.
[4] T. Viveros-García, J.A. Ochoa-Tapia, R. Lobo-Oehmichen, J.A. de los Reyes-Heredia, E.S. Pérez-Cisneros, Conceptual design of a reactive distillation process for ultra-low sulfur diesel production, Chem. Eng. J. 106 (2005) 119–131.

[5] E.S. Pérez-Cisneros, R. Gani, M.L. Michelsen, Reactive separation systems. I. Computation of physical and chemical equilibrium, Chem. Eng. Sci. 52 (4) (1997) 527–543.
[6] K.G. Joback, R.C. Reid, Estimation of pure-component properties from group contribution, Chem. Eng. Commun. 57 (1987) 223–243.
[7] D.H. Broderick, B.C. Gates, Hydrogenolysis and hydrogenation of dibenzothiophene catalyzed by sulfided CoO-MoO_3/γ-Al_2O_3: the reaction kinetics, AIChE J. 27 (4) (1981) 663–673.
[8] V. Vanrysselberghe, R.L. Gall, G.F. Froment, Hydrodesulfurization of 4-methyldibenzothiophene and 4,6-dimethyldibenzothiophene on a CoMo/γ-$A1_2O_3$ catalyst: reaction network and kinetics, Ind. Eng. Chem. Res. 37 (1998) 1235–1242.
[9] M. Houalla, N.K. Nag, A.V. Sapre, D.H. Broderick, B.C. Gates, Hydrodesulfurization of dibenzothiophene catalyzed by sulfided CoO-MoO_3/γ-Al_2O_3: the reaction network, AIChE J. 24 (6) (1978) 1015–1021.
[10] R. Shafi, G.J. Hutchings, Hydrodesulfurization of hindered dibenzothiophenes: an overview, Catal. Today 59 (2000) 423–442.
[11] G. Venimadhavan, G. Buzad, M.F. Doherty, M.F. Malone, Effect of kinetics on residue curve maps for reactive distillation, AIChE J. 40 (11) (1994) 1814–1824.
[12] D.Y. Peng, D.B. Robinson, A new two constant equation of state, Ind. Eng. Chem. Fundam. 15 (1976) 59–64.
[13] M.L. Michelsen, The isothermal flash problem. Part 1. Stability, Fluid Phase Equilibr. 9 (1982) 1–19.
[14] M.J. Girgis, B.C. Gates, Reactivities, reaction networks, and kinetics in high pressure catalytic hydroprocessing, Ind. Eng. Chem. Res. 30 (1991) 2021–2058.
[15] D.D. Whitehurst, T. Isoda, I. Mochida, Present state of the art and future challenges in the hydrodesulfurization of polyaromatic sulfur compounds, Adv. Catal. 42 (1998) 345–471.
[16] M. Breysse, G. Djéga-Mariadassou, S. Pessayre, C. Geantet, M. Vrinat, M. Pérot, M. Lemaire, Deep desulfurization: reactions, catalysts and technological challenges, Catal. Today 84 (2003) 129–138.
[17] J.M. Manoli, P. Da Costa, M. Brun, M. Vrinat, F. Maugé, C. Potvin, Hydrodesulfurization of 4,6-dimethyldibenzothiophene over promoted (Ni, P) alumina-supported molybdenum carbide catalysts: activity and characterization of active sites, J. Catal. 221 (2004) 365–377.
[18] R.H. Harrison, S.E. Scheppele, G.P. Sturm, P.L. Grizzle, Solubility of hydrogen in well-defined coal liquids, J. Chem. Eng. Data 30 (2) (1985) 183–189.